

“Wetting Enhancer” Pullulan Coating for Antifog Packaging Applications

Laura Introzzi,[†] José María Fuentes-Alventosa,^{†,‡} Carlo A. Cozzolino,^{†,§} Silvia Trabattoni,[‡] Silvia Tavazzi,[‡] Claudia L. Bianchi,[#] Alberto Schiraldi,[†] Luciano Piergiovanni,[†] and Stefano Farris^{*,†}

[†]DeFENS, Department of Food, Environmental and Nutritional Sciences, Packaging Division, University of Milan, Via Celoria 2, I – 20133 Milan, Italy

[‡]Centro de Investigación y Formación Agraria “Alameda del Obispo”, Instituto de Investigación y Formación Agraria y Pesquera (IFAPA), Avenida Menéndez Pidal s/n. 14004 Córdoba, Spain

[§]STAA, Department of Agriculture, University of Sassari, Viale Italia 39/A, I – 07100 Sassari, Italy

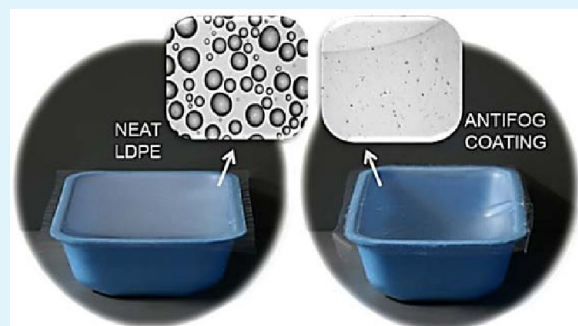
[‡]Department of Materials Science, University of Milano Bicocca, Via Cozzi 53, I – 20125 Milano, Italy

[#]Department of Chemistry, University of Milan, Via Golgi 19, I – 20133 Milano, Italy

S Supporting Information

ABSTRACT: A new antifog coating made of pullulan is described in this work. The antifog properties are discussed in terms of wettability, surface chemistry/morphology, and by quantitative assessment of the optical properties (haze and transparency) before and after fog formation. The work also presents the results of antifog tests simulating the typical storage conditions of fresh foods. In these tests, the antifog efficiency of the pullulan coating was compared with that of two commercial antifog films, whereas an untreated low-density polyethylene (LDPE) film was used as a reference. The obtained results revealed that the pullulan coating behaved as a “wetting enhancer”, mainly due to the low water contact angle ($\sim 24^\circ$), which in turn can be ascribed to the inherent hydrophilic nature of this polysaccharide, as also suggested by the X-ray photoelectron spectroscopy experiments. Unlike the case of untreated LDPE and commercial antifog samples, no discrete water formations (i.e., droplets or stains) were observed on the antifog pullulan coating on refrigeration during testing. Rather, an invisible, continuous and thin layer of water occurred on the biopolymer surface, which was the reason for the unaltered haze and increased transparency, with the layer of water possibly behaving as an antireflection layer. As confirmed by atomic force microscopy analysis, the even deposition of the coating on the plastic substrate compared to the patchy surfacing of the antifog additives in the commercial films is another important factor dictating the best performance of the antifog pullulan coating.

KEYWORDS: antifog, coating, packaging, pullulan, surface, wetting



INTRODUCTION

Current food packaging materials are conceived as a multifunctional tool enabling both the shelf life extension and the market penetration of food products. For this reason, besides containment, protection and preservation of foods, there is demand for packaging materials to afford additional properties, some of them not only directly related to food safety but also to a suitable presentation of the product.

One of these properties is the antifog property, which concerns the capability of the packaging material to avoid the forming small droplets of water on the internal side of the packaging film. Fog formation is a consequence of environmental changes in temperature and humidity: a decrease of film surface temperature below the dew point causes the condensation of water vapor present inside the package. The final effect is the appearance of a “foggy” layer that modifies the optical properties of the material, hiding the contents of the package by scattering of the incident

light in all directions, due the newly appeared droplets.¹ The nuisance of fogging on plastic films is frequently of concerns in the case of fresh food and minimally processed (washed, trimmed, sliced) vegetables, especially when they are refrigerated after packaging operations. The “see-through” property is actually one of the most important requirements of transparent films, as it can influence the final choice made by consumers. For this reason, it is important to preserve this property, as it can offer a more attractive display of the products throughout the shelf life of the packaged food.

It has been pointed out that the detrimental effect of fog on the transparency of the material mainly depends on the shape of the droplets,² which is reflected by the balance between the three

Received: May 4, 2012

Accepted: July 3, 2012

Published: July 3, 2012

interfacial energies (solid–liquid γ_{SL} , liquid–vapor γ_{LV} , and solid–vapor γ_{SV}) of the three-phase system, as described by Young's equation.³ The higher the contact angle, the higher the incident angle of the light normal to the substrate at the water/air interface, hence the more intense will be the scattering of the visible light. Not only the shape, but also the size of the droplets is another important factor to consider with regards to the antifog property of a material:² the smaller the size, the larger the number of droplets and the more pronounced the foggy effect. As both the shape and the size of the water droplets depend on the physicochemical characteristics of the substrate,⁴ modifying the original physicochemical properties of the plastic surface can be the key to controlling water droplet formation.⁵ Accordingly, most of the antifog packaging materials available on the market include additives (e.g., nonionic surfactants such as sorbitan esters, polyoxyethylene esters, glycerol esters, and more recently, polyglycerol esters) that migrate from the bulk to the surface of the plastic films, included with the goal of increasing the hydrophilic features of the hydrophobic surfaces of the materials commonly used in the food packaging field, especially polyolefins, such as polypropylene (PP) and polyethylene (PE).⁶

However, this approach involves two main disadvantages: (i) From a technical point of view, the fast migration of the additives imposes a quick use of the antifog films after manufacturing (i.e., very short warehousing). In addition, the antifog additives can be washed away from the film surface by the condensed vapor, which otherwise means that the claimed antifog properties tend to decrease over time. (ii) From a safety point of view, the migration of the additives onto the inner side of the packaging poses serious concerns in that they could transfer onto the food. This is generally seen as a potential health hazard, even though contamination is below the legislated limits. For the aforementioned reasons, it can be said that film manufacturers are still struggling with the fog formation problem and a suitable solution has not yet been found. Therefore, the development of high-performance, safe, and economical antifog solutions can be considered a still-open issue.

More recently, new alternative approaches have been suggested to achieve the antifog property. For example, Law et al.⁷ investigated the antifog properties of non-UV activated TiO₂ films, finding that surface roughness is the key parameter dictating the final antifog attribute. Patel et al. prepared superhydrophilic surfaces including both polyester films treated with oxygen plasma and indium tin oxide-coated glasses treated by an electrochemical method.⁸ Finally, Chiou et al. obtained films based on aligned polyaniline nanofibers with reversible superhydrophilic–superhydrophobic features by controlling the oxidation and reduction states by electrical potential.⁹ Of late, a new strategy has ventured into the use of coating technology to address the fog formation issue.^{10–12} Recent years have witnessed an increase in the development of a new generation of coatings intended for food packaging applications, the main distinctive feature lying in the use of at least one biopolymer as a main component. For example, sealing,^{13,14} oxygen barrier,¹⁵ and antimicrobial¹⁶ coatings have been produced according to this new trend. Also, antifog coatings, including at least one biopolymer rich in hydrophilic functionalities, have been recently designed.¹⁷ The basic working-principle of these coatings is to decrease the surface tension between the substrate and water, lowering the liquid contact angle and thus avoiding the formation of well-defined small droplets. The high hydrophilic character of the coating surface is the main reason why enhanced spreading of water droplets occurs on the surface, enabling the formation of a

continuous layer instead of a discrete pattern of fog drops. This, in turn, would prevent the scattering of the incident radiation.

In this work, we present a new antifog coating made of pullulan, an exopolysaccharide of biotechnological origin obtained from the yeast-like fungus *Aerobasidium pullulans*. Besides its well-known uses in the food industry, pullulan has been recently demonstrated to be a valid candidate for the development of functional coatings.^{4,15} In this paper, we discuss the antifog performance of pullulan coatings in comparison with some commercial antifog packaging films. To the best of our knowledge, this is the first work dealing with pullulan-based antifog coatings.

■ MATERIALS AND METHODS

Materials. Pullulan powder (PF-20 grade, $M_n \approx 200$ kDa) was provided by Hayashibara Biochemical Laboratories Inc. (Okayama, Japan). A hydro-alcoholic primer solution containing aziridine (0.5 wt %) was provided by Metalvuoto spa (Roncello, Milan, Italy). Corona-treated low-density polyethylene (LDPE) of $35 \pm 0.5 \mu\text{m}$ (Ticinoplast, Pogliano Milanese, Italy) was used as the plastic substrate for coating deposition. Two commercially available antifog films were used for comparison purposes: (i) PET/ink/tie/LDPE 60 μm thick, coded as AF_a (Carta Stampa srl, Briosco, Italy) and (ii) LDPE/EVOH/LDPE 70 μm thick, coded as AF_b (Castagna Univel spa, Guardamiglio, Italy). According to the information provided by the suppliers, both antifog LDPE layers were loaded (~ 0.5 wt %) with nonionic aliphatic OH-functional additives belonging to the polyglycerol esters family.

Preparation of the Antifog Coatings. A 2.5 wt % water solution of pullulan was first prepared by mixing the powdered polysaccharide with distilled water under slow stirring (200 rpm) at room temperature for 1 h. Besides the surface activation of the LDPE substrate by the corona treatment, to enhance the adhesion between substrate and coatings a thin layer of primer (0.5 wt % aziridine homopolymer water/ethanol solution) was laid onto the LDPE surface by means of an automatic film applicator (Ref. 1137, Sheen Instruments, Kingston, UK) equipped with a steel horizontal rod with an engraved pattern, enabling the deposition of a layer of 4.0 μm thickness (wet basis). Solvent evaporation was performed using a constant and perpendicular flux of mild air (25.0 ± 0.3 °C for 2 min) at a distance of 40 cm from the applicator. Afterward, a first layer of the pullulan water solution was applied by means of a rod enabling the deposition of a wet thickness of 10.0 μm (i.e., a theoretical dry thickness of 0.25 μm , given the 2.5 wt % pullulan water solution). After solvent removal, a second layer of pullulan was applied according to the aforementioned procedure, thereby achieving a final antifog thickness of $\sim 0.5 \mu\text{m}$. The deposition of both primer and antifog coating was performed at a constant speed of 2.5 mm s^{-1} , according to ASTM D823–07 – Practice C.

Contact Angle Measurements. Contact angle measurements were performed on neat LDPE (corona-untreated side), pullulan antifog coating (AF_{pull}), and the two commercial antifog films: AF_a and AF_b. For this purpose an optical contact angle apparatus (OCA 15 Plus, Data Physics Instruments GmbH, Filderstadt, Germany) was used, equipped with a high-resolution CCD camera and a high performance digitizing adapter. SCA20 and SCA21 software (Data Physics Instruments GmbH, Filderstadt, Germany) were used, respectively, for contact angle measurements and surface energy calculation. Rectangular ($5 \times 2 \text{ cm}^2$) specimens were fixed and kept flat throughout the analysis by means of a special sample holder with parallel clamping jaws.

The static contact angle of water in air (θ , deg) was measured by the sessile drop method, by gently dropping a droplet of $4.0 \pm 0.5 \mu\text{L}$ of Milli-Q water ($18.3 \text{ M}\Omega \text{ cm}$) onto the substrate, according to the so-called pick-up procedure (a droplet hanging down from the needle is laid on a solid surface by raising the sample stage until solid/liquid contact is made) at 23 ± 1 °C and $50 \pm 2\%$ relative humidity (RH). All droplets were released from a height of 1 cm above the surface to ensure consistency between each measurement. The static contact angle was measured immediately after droplet deposition as the angle between the baseline of the drop and the tangent at the drop boundary. However, it

has been previously demonstrated that for pullulan coatings, the equilibrium contact angle for polar liquids (e.g., water) is achieved with good approximation after 60 s upon deposition of the droplet, because of the strong hydrophilic nature of the biopolymer surface.⁴

Advancing contact angle measurements were also performed with the goal of gathering information on the homogeneity of the antifog distribution on the plastic substrate. This was accomplished through the sessile drop “needle-in” method: 0.15 μL of the liquid was continuously dispensed onto a 2 μL droplet previously deposited on the film surface, at a rate of 1 $\mu\text{L s}^{-1}$. The advancing contact angle (θ_{adv}) was then considered as the angle measured at the plateau of the θ (deg) versus time (s) plot.

Finally, a quantitative determination of the surface thermodynamic properties of the different substrates was performed using the Van Oss' adaptation of Young's theory¹⁸

$$(1 + \cos \theta)\gamma_L = 2(\sqrt{\gamma_S^{\text{LW}}\gamma_L^{\text{LW}}} + \sqrt{\gamma_S^+ \gamma_L^-} + \sqrt{\gamma_S^- \gamma_L^+}) \quad (1)$$

where θ = contact angle (deg), γ_L = surface tension of the liquid in contact with the solid surface (mJ/m^2), γ_L^{LW} = apolar component (LW) of the surface tension of the liquid (mJ/m^2), γ_L^+ = electron-acceptor parameter of the polar component (AB) of the liquid (mJ/m^2), γ_L^- = electron-donor parameter of the polar component (AB) of the liquid (mJ/m^2), γ_S^{LW} = apolar component (LW) of the surface energy of the solid (mJ/m^2), γ_S^+ = electron-acceptor parameter of the polar component (AB) of the solid (mJ/m^2), γ_S^- = electron-donor parameter of the polar component (AB) of the solid (mJ/m^2)

From eq 1, it is possible to calculate the surface energy of the solid (γ_S), according to the following relationship

$$\gamma_S = \gamma_S^{\text{LW}} + \gamma_S^{\text{AB}} \quad (2)$$

where γ_S^{AB} is the polar (AB) surface energy component of the solid surface (mJ/m^2) calculated with the following expression

$$\gamma_S^{\text{AB}} = 2\sqrt{\gamma_S^+ \gamma_S^-} \quad (3)$$

Because γ_L , γ_L^{LW} , γ_L^+ , and γ_L^- were known,¹⁹ the three thermodynamic parameters (i.e., γ_S^{LW} , γ_S^+ , and γ_S^-) related to the solid surfaces were determined by measuring the θ of three different liquids, two polar (i.e., water and formamide) and one apolar (i.e., diiodomethane) (Table 1).

Table 1. Surface Tension Components (γ_L^{LW} and γ_L^{AB}) and Parameters of γ_L^{AB} (γ_L^+ and γ_L^-) for Water, Formamide, and Diiodomethane in mJ/m^2 at 20 °C^a

liquid	thermodynamic parameter				
	γ_L	γ_L^{LW}	γ_L^{AB}	γ_L^+	γ_L^-
water	72.8	21.8	51.0	25.5	25.5
formamide	58.0	39.0	19.0	2.28	39.6
diiodomethane	50.8	50.8	0	≈ 0.01	0

^aAdapted from van Oss (2003).¹²

Atomic Force Microscopy (AFM). The surface morphology of the corona-untreated side of neat LDPE, the antifog pullulan coating, and the antifog side of samples AF_a and AF_b were all analyzed using a Nanoscope V MultiMode (Veeco) in tapping mode. Measurements were carried out in air using a silicon tip (resonance frequency 287–346 kHz, spring constant 20–80 N/m). The images were recorded with a resolution of 512 \times 512 pixels and corrected using a second-order polynomial background filter. The root-mean-square roughness S was also evaluated for each sample as the standard deviation of the topography over the 30 \times 30 μm^2 scanning area ($M \times N$ pixels)

$$S = \sqrt{\frac{1}{MN} \sum_{i=1}^M \sum_{j=1}^N |z(x_i, y_j) - \bar{z}|^2} \quad (4)$$

where \bar{z} is the mean value of the topography $z(x,y)$.

X-ray Photoelectron Spectroscopy (XPS). XPS measurements were performed in an M-Probe Instrument (Surface Science Instruments, Uppsala, Sweden) equipped with a monochromatic Al K α source (1486.6 eV) with a spot size of 200 \times 750 μm and a pass energy of 25 eV, providing a resolution of 0.74 eV. The energy scale was calibrated with reference to the 4f_{7/2} level of a freshly evaporated gold sample, at 84.0 \pm 0.1 eV, and with reference to the 2p_{3/2} and 3s levels of copper at 932.47 \pm 0.1 and 122.39 \pm 0.15 eV, respectively. With a monochromatic source, an electron flood gun was used to compensate for the buildup of positive charge on the insulator samples during the analyses: a value of 10 eV was selected to perform measurements on these samples. For all the samples, the C_{1s} peak level was taken as internal reference at 284.6 eV. The accuracy of the reported binding energies (BE) can be estimated to be ± 0.2 eV. The quantitative data were also accurately checked and reproduced several times and the percentage error was estimated to be $\pm 1\%$ thanks to a severe confidence level in spectral decomposition.

Optical Microscopy. Water droplet morphology and organization of both untreated LDPE and antifog films (AF_a, AF_b, and AF_{pull}) were visualized using an optical microscope (OM) (Micro Nikon Eclipse ME600 Laboratory Imaging; Nikon Instruments, Sesto Fiorentino, Italy) at 10 \times magnification. Pieces of film (30 \times 10 mm²) were mounted on a rectangular glass sample holder immediately after storage in the refrigerator and observed without any pretreatment. Image capture was carried out using NIS-Element software (Nikon Instruments, Sesto Fiorentino, Italy).

Antifog Test. The antifog properties of pullulan coatings were evaluated by simulating real storage conditions of many refrigerated fresh foods. In other words, water was trapped in a closed system and the temperature was lowered down below the dew point to allow for the formation of droplets (fog) on the polymer surface due to condensation. For this purpose, expanded polystyrene (EPS) trays (Sirap Gema, Verolanuova, Italy) previously filled with 50 mL of distilled water were hermetically sealed (top surface area 215 \times 125 mm²) with the LDPE pullulan-coated films using a vacuum/gas sealing machine (mod. Quick, Tecnovac srl, Grassobbio, Italy) at room temperature. For comparison, the same trays were also sealed with bare LDPE and the two commercial antifog films. The trays were then placed in a refrigerator (4.0 \pm 0.5 °C, 90 \pm 2% RH) for 7 days. Water droplet formation was monitored daily by visual inspection. Photographs were taken immediately after drawing the trays out from the cold chamber into the laboratory environment (~ 20 °C).

Optical Properties. To assess quantitatively the antifog properties of the different films, haze was measured in accordance with ASTM D 1003–00, using a UV–vis high-performance spectrophotometer (Lambda 650, PerkinElmer, Waltham, MA, USA) coupled with a 150 mm integrating sphere, which allows trapping of the diffuse transmitted light. Quantification of haze, defined as the percentage of transmitted light deviating by more than an angle of 2.5° from the direction of the incident beam, is important, especially from a commercial point of view, as it is responsible for the reduction in the contrast between objects viewed through the specimen (e.g., the coated plastic film).

Transparency was assessed in accordance with the ASTM D 1746–88 using a UV–vis high-performance spectrophotometer (Lambda 650, PerkinElmer, Waltham, MA, USA) in a “sphere-less” configuration. Transparency was measured in terms of specular transmittance (i.e., the transmittance value obtained when the transmitted radiant flux includes only the light transmitted in the same direction as that of the incident flux at a 550 nm wavelength).

Ten replicates were made for each uncoated and coated film sample in both analyses.

Statistical Analysis. The statistical significance of differences between samples was determined by one-way analysis of variance (ANOVA), using JMP 5.0.1 software (SAS Campus Drive, Cary, NC). The mean values, where appropriate, were compared by Student's *t*-test with a significance level (*p*) < 0.05.

RESULTS AND DISCUSSION

Wettability, Surface Energy Determination, and Surface Morphology. Results arising from the contact angle

Table 2. Static Contact Angles (θ , deg), Surface Energy Components (γ_s^{LW} and γ_s^{AB} , mJ/m²), and Parameters of γ_s^{AB} (γ_s^+ and γ_s^- , mJ/m²) for the Films Tested in This Work

solid	thermodynamic parameter							
	$\theta_{(w)}^a$	$\theta_{(f)}^a$	$\theta_{(d)}^a$	γ_s	γ_s^{LW}	γ_s^{AB}	γ_s^+	γ_s^-
LDPE	89.20 ± 1.03	68.96 ± 1.22	60.52 ± 1.67	30.28 ± 1.77	28.28 ± 0.96	1.99 ± 0.11	0.29 ± 0.07	3.42 ± 0.77
AF _a	52.08 ± 3.17	39.49 ± 3.28	47.49 ± 4.88	46.01 ± 7.01	35.66 ± 2.67	10.36 ± 0.11	1.03 ± 0.67	26.04 ± 4.79
AF _b	39.22 ± 17.39	68.19 ± 3.27	56.21 ± 9.51	30.41 ± 5.19	30.41 ± 5.42	0.00 ± 0.00	0.00 ± 0.00	80.11 ± 33.0
AF _{pull}	24.06 ^b ± 0.92	23.39 ^b ± 1.25	53.77 ± 0.41	53.58 ± 1.31	32.15 ± 0.23	21.43 ± 0.12	2.33 ± 0.18	49.30 ± 1.16

^aw = water; f = formamide; d = diiodomethane. ^bContact angle values at time = 60 s.

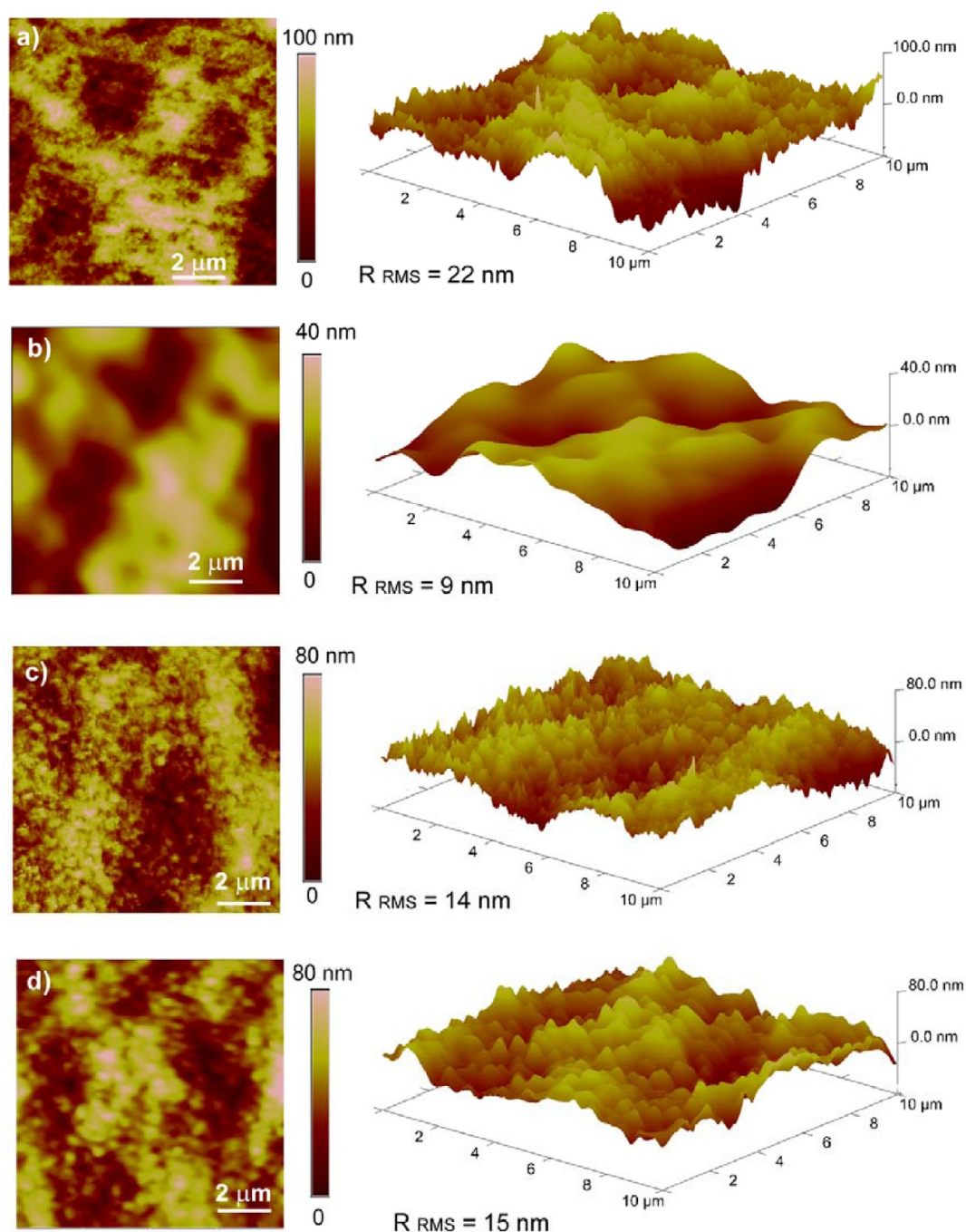


Figure 1. AFM height and 3D images (10 × 10 μm²) of (a) the untreated LDPE and the antifog coatings (b) AF_{pull}, (c) AF_a, and (d) AF_b.

analyses are summarized in Table 2. The three antifog films exhibited lower static water contact angle values (first column on the left) than the neat LDPE substrate, suggesting that the

antifog treatment (both the pullulan coating and the antifog additives) were effective at increasing the wettability of the inherently hydrophobic plastic surface. However, the best

performance in this respect was provided by the pullulan coating ($\theta \sim 24^\circ$) compared with the AF_b ($\theta \approx 39^\circ$) and AF_a ($\theta \approx 52^\circ$) samples. A more in-depth observation also reveals quite a high spreading of the experimental θ data around the mean value for the AF_b sample, presumably owing to the less homogeneous distribution of the antifog additive at the solid/air interface.

The AFM images displayed in Figure 1 clearly show different surface morphologies for the neat LDPE substrates and the antifog coatings AF_a , AF_b , and AF_{pull} . As a general trend, the presence of the antifog coatings led to an increase in smoothness, with the pullulan antifog coating exhibiting the best “flattening” performance compared to a more “stainlike” pattern for the commercial samples. These different topographies would eventually affect the wetting behavior of the water droplets. The advancing contact angle data provided a first indication of this. As can be seen in Figure 2, the θ_{adv} versus time profile of the

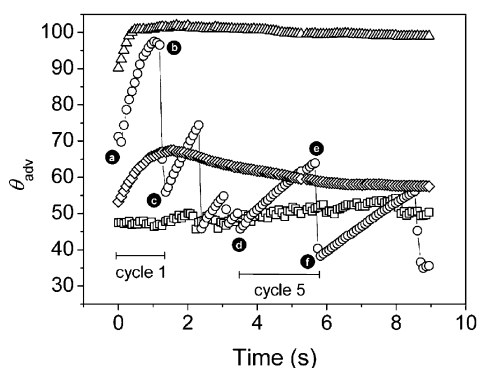


Figure 2. Advancing water contact angle evolution for the corona-untreated LDPE side (Δ), the antifog pullulan coating (\diamond), and the commercial antifog films AF_a (\square) and AF_b (\circ) over a 10 s time span.

sample AF_b sample shows jagged spikes compared to the more regular pattern observed for the neat LDPE substrate and the pullulan coating. The commercial antifog film AF_a disclosed a slightly “noisy” behavior, though with peaks of decidedly smaller size compared with the sample AF_b .

The peculiar behavior observed for the AF_b sample can be better understood considering the interaction between the “advancing” water droplets and the film surface (Figures 2 and 3): at the beginning ($t < 2$ s) (Point *a* in Figures 2 and 3a), as more water was dispensed, the volume increase caused a symmetric increase in θ_{adv} (i.e., the left and right advancing contact angles increased proportionally) (Point *b* in Figures 2 and 3b). At a certain point, as soon as the water molecules met a

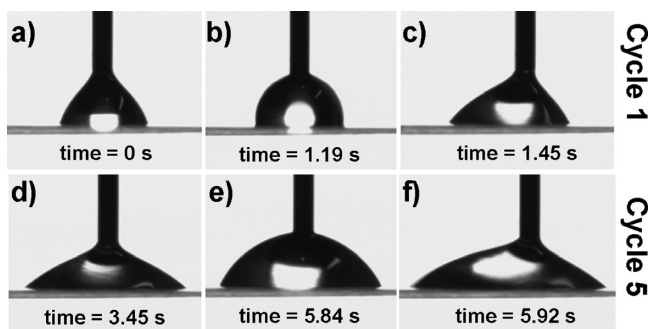


Figure 3. Frames captured for the advancing water contact angle experiment on the AF_b antifog film. Note the skewed shape of the water droplet in frames *c* and *f*.

more hydrophilic area (i.e., the antifog additive), the wettability increased visibly (i.e., the θ_{adv} decreased). However, owing to the patchy surfacing of the antifog additive, the water droplet appeared skewed on one side (Point *c* in Figure 2 and Figure 3c). This asymmetry tended to disappear gradually on further solvent dispensation, to take place again as a new antifog area was encountered.

Several “growth–collapse” cycles of the water droplet were observed on the AF_b surface during the advancing contact angle experiments (see Supporting Information—media video), to which corresponded different thermodynamic metastable states, each state producing a given contact angle. The AF_{pull} coating exhibited a different profile: following a maximum θ_{adv} value (after ~ 1.5 s), θ_{adv} decreased monotonically over time. This was demonstrated to be due to the considerable spreading phenomenon of water on the hydrophilic surface of pullulan.⁴ The more homogeneous covering of the pullulan coating on the plastic substrate, as also revealed by the AFM images (Figure 1), explains why the θ_{adv} evolution did not show a ‘step-like’ profile as in the case of the AF_b sample. This is the key-factor behind the antifog properties of pullulan allowing water to spread easily, thus enabling the formation of a continuous thin layer instead of individual droplets on the plastic film. This, in turn, prevents the scattering of incident light (i.e., the fog-induced optical artifacts).

Relevant considerations also arose from the surface energy calculation of the four different films (Table 2). While both the pullulan antifog coating and the commercial antifog film AF_a showed higher γ_s compared to the bare, untreated LDPE surface, the AF_b sample disclosed a γ_s value as low as that of the neat plastic film (~ 30 mJ/m²). This apparently strange behavior of the AF_b sample can be explained considering the two components (i.e., polar and apolar) of the total surface energy value. More specifically, it can be seen that the antifog treatment (both in the form of coating deposition and additive migration on the surface) led to a marked increase in the electron-donor parameter (γ^-) of the polar component (γ^{AB}) for the three antifog materials in comparison with the neat LDPE substrate. On the contrary, the electron-acceptor (γ^+) parameter increased to a very limited extent for the AF_{pull} and AF_a samples, and was equal to zero for the AF_b sample. Because eq 3 applies between γ^- and γ^+ , the polar component for the AF_b sample becomes void. This is why, given the total surface energy (γ_s) expressed by the eq 2, it has been verified that $\gamma_s = \gamma^{LW}$ for the AF_b sample. These results suggest that, for the three antifog samples, the antifog property induced on the LDPE substrate must be attributed exclusively to the electron-donor parameter of the polar component. Pullulan, in particular, behaved as most solid, polar, nonionic hydrophilic surfaces (i.e., as a strong monopolar electron donor with a γ -value similar to values encountered for synthetic polymers such as poly(ethylene oxide) (PEO) and poly(vinyl alcohol) (PVOH)).¹⁸

As far as the antifog pullulan coating is concerned, the surface energy analysis yielded values of the different components and parameters slightly different from those reported previously.⁴ Most probably, the reason lies in the different substrates used for the coating deposition (i.e., primed LDPE instead of corona-treated PET). This would have promoted different interactions at the substrate/biopolymer interface, hence a different structuring of pullulan on the plastic surface.²⁰ From these findings, it can be said that considering the components of the surface energy (γ^{LW} and γ^{AB}) rather than the total surface energy value as a whole (γ_s) is a more appropriate approach for

explaining the thermodynamic equilibrium of water in a realistic way.

X-ray Photoelectron Spectroscopy (XPS). The surface chemical compositions of untreated LDPE, corona-treated LDPE (LDPE_{corona}), and the antifog coatings AF_a, AF_b, and AF_{pull} were determined by XPS. As shown in Table 3, from XPS

Table 3. Summary of XPS Measurements

sample	% C	% O	% Si	O/Si
LDPE	82.3 ± 3.2	10.8 ± 1.1	6.9 ± 0.6	1.57
LDPE _{corona}	78.5 ± 4.8	13.9 ± 1.4	7.7 ± 0.7	1.81
AF _a	77.8 ± 5.4	14.2 ± 2.1	8.1 ± 1.2	1.75
AF _b	75.1 ± 5.1	15.8 ± 2.3	9.1 ± 1.4	1.74
AF _{pull}	89 ± 4.4	6.8 ± 0.3	4.2 ± 0.2	1.62

spectra, it was possible to draw information about the atomic composition of the surface, essentially in terms of carbon and oxygen atoms. Nevertheless, we also detected a fairly high (although variable) amount of silicon on the surface of all samples. Although unexpected, this result has already been reported in previous works, where the presence of silicon on the surface of polyolefins was primarily ascribed to the presence of additives that had migrated from the bulk, such as synthetic and natural silica, which are used in elevated levels as antiblocking agents to decrease the coefficient of friction of the film.²¹ However, contamination of the surface due to silicon grease cannot be excluded.²²

The presence of Si on the surface made it difficult to acquire direct information on the chemical surface changes induced by the different treatments (corona, primer, antifog additives, and coating deposition). The overall increase in the amount of oxygen while increasing the amount of silicon confirms that part of the oxygen is most likely due to the mineral filler and contaminants. However, it can be assumed that a comparable silicon content lies on the surface of different LDPE films (an assumption that actually holds true for LDPE layers of a same origin, i.e., for the sample LDPE, LDPE_{corona}, LDPE_{primer}, and AF_{pull}). Under this assumption, a crude estimate of the entity of the possible changes in surface chemistry that occurred on the surface-treated samples (LDPE_{corona}, LDPE_{primer}, AF_a, AF_b, and AF_{pull}) can be done considering the oxygen/silicon atomic ratio (O/Si) parameter. As reported in Table 3 (fifth column), the lowest O/Si value is for the bare LDPE, according to a prevalently aliphatic backbone (CH₂–CH₂)_n. Conversely, the highest O/Si value is observed for the corona-treated LDPE substrate, as a consequence of the oxidation of the main hydrocarbon backbone by the physical treatment. More specifically, it has been pointed out that the most representative oxygen-based polar groups introduced on the corona-treated polyethylene surfaces are: i) carbon carrying hydroxyl groups (C–OH); ii) carbonyl groups (C=O); and iii) carboxyl groups (COOH).²³ The corresponding increase in the percentage of Si can be tentatively explained by the physical damages induced by the corona treatment on the plastic polymer,²⁴ which would have boosted the surfacing of the silica filler. As far as the other samples are concerned, it can be seen that the commercial antifog films have a similar O/Si value, which is however higher compared with the bare LDPE, reflecting the abundance of –OH groups in the antifog additives that had migrated to the surface. The highest percentage of Si values recorded for both AF_a and AF_b samples can reasonably account for the different origin of the LDPE films, which could have

undergone different (in terms of type and intensity) surface activation treatments (e.g., corona, plasma, and flame treatments) that, in turn, might have increased the amount of silica exposed on the surface. Finally, the O/Si value for the pullulan-coated LDPE surface was not as high as expected. This finding can be explained considering two different effects: (i) the coating deposition partially masked the silica atoms on the surface, thus the decrease in both the percentage of Si and the percentage of O; (ii) although new functional polar groups (i.e., –OH groups of pullulan) have been added to the LDPE surface, the deposition of the coating led to a concomitant increase in the amount of the carbon atoms, which account for the highest percentage of C atoms recorded (89%).

Arising from the XPS results, it can be reasonably suppose that, following the physical (corona) and chemical (primer) activation treatments, the presumed bonding between substrate (LDPE) and coating (pullulan) should take place according to the scheme reported in Figure 4. Here, it can be seen that the new adhesion forces (mainly hydrogen bonds and ion-dipole interactions) would occur between the new established polar groups on the polyolefin backbone and the hydroxyl pendant groups of pullulan.

Antifog Test. To assess the antifog efficiency of the AF_{pull} coating, tray samples were stored for 7 days under refrigerated conditions (~4 °C), much as fresh foods such as minimally processed vegetables. The same experiments were simultaneously conducted on both the neat LDPE substrate and the commercial antifog films, to check for any possible differences in the ultimate antifog properties between the commercial and AF_{pull} samples.

Although the four samples had different starting optical properties in terms of either haze or transparency or both (Table 4, *t* = 0 days), transparency was high enough to guarantee that the freshly sealed trays looked equally good, enabling a see-through quality for the package, as displayed in Figure 5a. It is worth noting that at *t* = 0 days, the optical properties (both haze and transparency) of LDPE and AF_{pull} were found to be very similar. A detailed analysis of the values indicates that the pullulan-coated samples exhibited transparency and haze values slightly larger and lower, respectively, than the neat LDPE. Even if weak, these differences can typically be recognized in the samples by the naked eye. They are attributable to the smoothing of the original LDPE surface by the pullulan coating. Indeed, both the roughness values and the lateral size of the surface structures (Figure 1a, b) are compatible with light scattering due to surface roughness effects, while the intensity of the scattered light is roughness-dependent.^{25–27} This attribution of the lower haze and increased transparency to the reduced surface roughness is also compatible with results reported in the literature for similar systems,^{28,29} showing that increased values of roughness are responsible for a rise in the component of the total haze related to the surface scattering. In particular, for polyolefin thin films (<50 μm in thickness), surface scattering has been demonstrated to represent the main component of the measured haze.³⁰ After storage in the refrigerator, the differences between trays became even more pronounced and the scenario changed dramatically. Very small water droplets formed on the untreated LDPE film, which exhibited a marked homogeneous foggy layer. This was responsible for the dramatic haze rise (almost 6 fold increase), to which corresponded a depletion in transparency of the final package (~66% decrease). The antifog additives provided a marked improvement in the commercial films, with the increase in haze after 7-days storage at 4 °C not statistically different

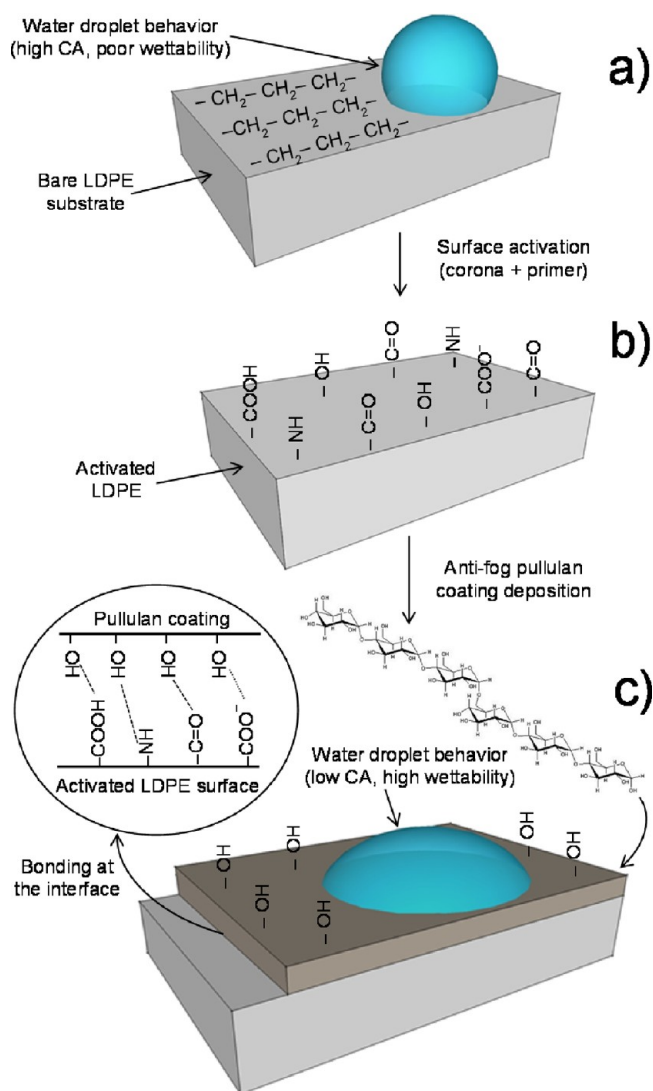


Figure 4. (a) Surface modifications occurred on the bare LDPE substrate; (b) after activation by corona discharge and primer; and (c) after the deposition of the antifog pullulan coating. A schematic representation of the presumed bonding mechanism between the activated LDPE substrate and the pullulan coating is provided in the inset. Also note the water droplet behavior before and after coating deposition.

compared with the original haze value ($\sim 10\%$ for both the AF_a and AF_b samples). However, a visual inspection clearly revealed the formation of well-defined water patches, especially for the AF_a sample, as can be seen in Figure 5. Even if the water patches do not substantially change haze, they are expected to refract the light (as water optical lenses). This was reflected in the final

transparency recorded for the two commercial samples, particularly for AF_a (Table 4). After storage in the refrigerator, the antifog film AF_a , despite its higher initial transparency ($\sim 77\%$), exhibited a final value approximately 10% lower than the AF_b sample, which actually kept its original transparency almost unaltered. This decrease cannot be attributed to the increase in haze (Table 4), but is attributed to light refraction due to water lenses.

Concerning the AF_{pull} sample, no statistical difference was observed in the haze values after storage, whereas the statistical difference in transparency suggests that the formation of a continuous layer of water had a positive effect (Table 4). This positive effect occurred for the antireflection behavior of the water layer. Indeed, the water layer has an intermediate refractive index ($n = 1.33$) with respect to pullulan and air refractive indices. Therefore, the antireflection behavior of the water layer occurs when its thickness is equal to $[(2j + 1)\lambda]/(4n)$, with $j = 0, 1, 2, \dots$, namely about 103, 310, 517, 724 nm, and so on. The calculated transmittance and reflectance for normal-incident light on a stack formed by a bulk material with refractive index equal to 1.50 and a top layer with refractive index $n = 1.33$ are reported in Figure 6. The top layer produces antireflection behavior for the above-mentioned thickness values. The calculated transmittance can reach values larger than 95% for a proper top-layer thickness, but the calculations do not take haze losses into consideration. Given that haze for the diffused transmitted light has been measured to be about 6%, the total haze (both transmitted and reflected diffused light) is expected to be approximately 12%. This amount is in reasonable agreement with the difference between the measured 85% value and the calculated 95% one.

The antifog tests unequivocally indicated that the trays with the antifog pullulan coating clearly exhibited the best final overall display. Water deposition in these trays produced neither a significant increase in the haze nor a loss of transmittance due to the possible effects of water lenses, whereas it possibly produced an increase of transmittance when the thickness of the water layer matched the antireflection conditions. These results demonstrate that the deposition of the pullulan coating allowed for preserving the original optical properties of the substrate very efficiently (Figure 5b).

To provide an exhaustive explanation of the observed behaviors, we acquired some OM images of the four different samples immediately after removal from the 7-day storage in the refrigerator (Figure 7). The untreated LDPE substrate (Figure 7a) disclosed a peculiar pattern of discrete droplets of small size. The size, though of secondary importance relative to the contact angle of the droplet, is an important factor to consider when discussing the antifog behavior of different substrates. It is generally recognized that the smaller the size, the higher the scattering of the incident light.² It was experimentally demonstrated that, with good approximation, the boundary

Table 4. Haze and Transparency of Untreated LDPE, the Two Commercial antifog Samples (AF_a and AF_b), and the Pullulan antifog Sample (AF_{pull}) before ($t = 0$) and after 7 days ($t = 7$) of Storage in the Refrigerator at $\sim 4^\circ C^a$

sample	haze (%)		transparency (%)	
	$t = 0$ days	$t = 7$ days	$t = 0$ days	$t = 7$ days
LDPE	6.06 ± 0.11^a	46.78 ± 5.07^d	82.60 ± 0.62^A	27.56 ± 2.43^E
AF_a	10.08 ± 0.56^b	11.69 ± 1.54^b	77.82 ± 0.46^B	63.13 ± 13.09^{BF}
AF_b	9.92 ± 0.13^b	12.26 ± 1.99^b	72.85 ± 0.58^C	72.25 ± 4.28^{CFG}
AF_{pull}	5.40 ± 0.23^c	6.09 ± 0.58^c	84.44 ± 1.22^D	85.24 ± 1.05^G

^aSuperscripts denote a statistically significant difference within and between groups for each response ($p < 0.05$).

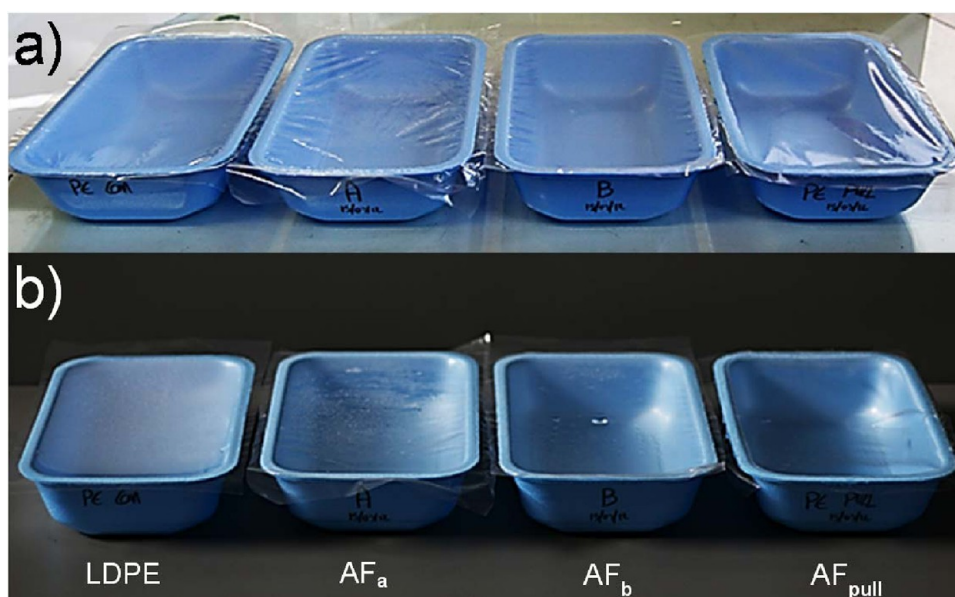


Figure 5. Untreated LDPE, commercial antifog samples (AF_a and AF_b), and pullulan antifog sample (AF_{pull}) (a) immediately before storage and (b) after removal from the refrigerator (7 days at ~ 4 °C) into the laboratory environment (~ 20 °C).

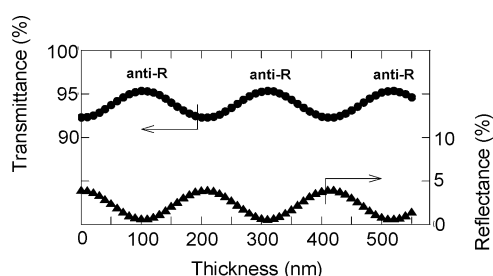


Figure 6. Calculated transmittance and reflectance for normal-incident light on a stack formed by a bulk material with refractive index equal to 1.50 and a top layer with refractive index $n = 1.33$ and variable thickness.

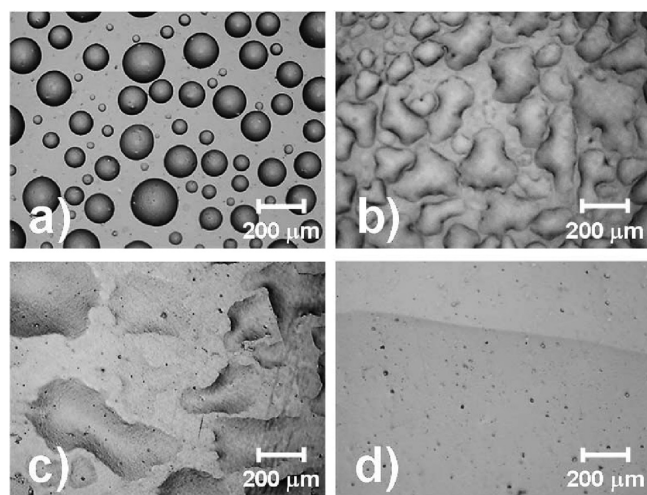


Figure 7. OM images (10 \times) of (a) untreated LDPE, commercial antifog (b) AF_a and (c) AF_b , and pullulan antifog coating (d) AF_{pull} immediately after removal from the 7-day storage in the refrigerator at 4 °C.

value is 1 mm (i.e., droplets of average diameter less than 1 mm—as in the case of the untreated LDPE—should be considered “fog-forming”).³¹

Some differences were detected between the two commercial samples. The AF_a sample (Figure 7b) exhibited a denser concentration of water “islands” of smaller size compared with the AF_b sample (Figure 7c). Nevertheless, for both samples, the observed “islands” were flat enough not to jeopardize the original haze of the film, considering that for droplets of low contact angle, the total internal reflection phenomenon of the incident light rays is deemed negligible.² As a matter of fact, it can thus be said that both commercial antifog films were effective at preventing increased haze arising from the fog formation. However, they behaved differently from an aesthetic point of view, as the formation of discrete stains of water was more pronounced for the AF_a sample. As already mentioned, the reduced transparency of AF_a is attributable to the effect of water lenses. The larger contact angle of AF_a (Table 2) and the images in Figure 7 further support this interpretation, given that refraction is more pronounced for a larger lens curvature. The best antifog performance aspect of the AF_{pull} sample is in the extensive spreading of water on the pullulan coating surface, as depicted in Figure 7d. None of the discrete water formation previously described (i.e., droplets or stains) was detected on the pullulan coating surface, suggesting that this polysaccharide acted as an effective “wetting enhancer” that pushed the condensed water molecules to form a continuous thin layer.

CONCLUSIONS

A new coating based on pullulan with outstanding antifog properties was prepared for the first time. The obtained results clearly showed that the homogeneous deposition of pullulan throughout the surface of the plastic film beneath played a pivotal role in dictating better overall performance compared with two commercial antifog films. The findings arising from this work may represent an advance in the still-unsolved issue of fog formation on plastic films, especially those intended for food packaging applications (e.g., polyolefins). Indeed, pullulan coatings may be of significant importance as a better, new and “green” alternative to conventional antifog additives in future applications.

■ ASSOCIATED CONTENT

● Supporting Information

Optical contact angle video showing the dynamic metastable wetting behavior of a commercial antifog packaging film. This material is available free of charge via the Internet at <http://pubs.acs.org>.

■ AUTHOR INFORMATION

Corresponding Author

*Tel.: +39 0250316654. Fax: +39 0250316672. E-mail: stefano.farris@unimi.it (S. Farris).

Notes

The authors declare no competing financial interest.

■ REFERENCES

- (1) Grosu, G.; Andrzejewski, L.; Veilleux, G.; Ross, G. G. *J. Phys. D: Appl. Phys.* **2004**, *37*, 3350–3355.
- (2) Howarter, J. A.; Youngblood, J. P. *Macromol. Rapid Commun.* **2008**, *29*, 455–466.
- (3) Young T. *Philos. Trans. R. Soc. London* **1805**; Vol. 95, pp 65–87.
- (4) Farris, S.; Introzzi, L.; Biagioni, P.; Holz, T.; Schiraldi, A.; Piergiovanni, L. *Langmuir* **2011**, *27*, 7563–7574.
- (5) Cebeci, F. C.; Wu, Z.; Zhai, L.; Cohen, R. E.; Rubner, M. F. *Langmuir* **2006**, *22*, 2856–2862.
- (6) Plasman, V.; Caulier, T.; Boulos, N. *Plast. Addit. Compd.* **2005**, *7*, 30–33.
- (7) Law, W. S.; Lam, S. W.; Gan, W. Y.; Scott, J.; Amal, R. *Thin Solid Films* **2009**, *517*, 5425–5430.
- (8) Patel, P.; Choi, C. K.; Meng, D. D. *J. Assoc. Lab. Automat.* **2010**, *15*, 114–119.
- (9) Chiou, N.-R.; Lu, C.; Guan, J.; Lee, L. J.; Epstein, A. J. *Nat. Nanotechnol.* **2007**, *2*, 354–357.
- (10) Chevallier, P.; Turgeon, S.; Sarra-Bournet, C.; Turcotte, R.; Laroche, G. *ACS Appl. Mater. Interfaces* **2011**, *3*, 750–758.
- (11) Maechler, L.; Sarra-Bournet, C.; Chevallier, P.; Gherardi, N.; Laroche, G. *Plasma Chem. Plasma Process.* **2011**, *31*, 175–187.
- (12) Paleari, M.; Cantoni, R.; Perego, V. U.S. 2010/0034928 A1, 2011.
- (13) Farris, S.; Cozzolino, C. A.; Introzzi, L.; Piergiovanni, L. *Packag. Technol. Sci.* **2009**, *22*, 359–369.
- (14) Farris, S.; Cozzolino, C. A.; Introzzi, L.; Piergiovanni, L. *J. Appl. Polym. Sci.* **2010**, *118*, 2969–2975.
- (15) Farris, S.; Introzzi, L.; Fuentes-Alventosa, J. M.; Santo, N.; Rocca, R.; Piergiovanni, L. *J. Agric. Food Chem.* **2012**, *60*, 782–790.
- (16) Pérez-Pérez, M. C.; Regalado-González, C.; Rodríguez-Rodríguez, C. A.; Barbosa-Rodríguez, J. R.; Villaseñor-Ortega, F. In *Advances in Agricultural and Food Biotechnology*; Guevara-González, R. G. Torres-Pacheco, I., Eds.; Research Signpost: Kerala, India, 2006; pp 193–216.
- (17) Nuraje, N.; Asmatulu, R.; Cohen, R. E.; Rubner, M. F. *Langmuir* **2011**, *27*, 782–791.
- (18) Van Oss, C. J. In *Interfacial Forces in Aqueous Media*; Marcel Dekker: New York, 1994; pp 21–22, 89–107.
- (19) Van Oss, C. J. *J. Mol. Recognit.* **2003**, *16*, 177–190.
- (20) Harnett, E. M.; Alderman, J.; Wood, T. *Colloids Surf., B* **2007**, *55*, 90–97.
- (21) Peloso, C. W.; O'Connor, M. J.; Bigger, S. W.; Scheirs, J. *Polym. Degrad. Stab.* **1998**, *62*, 285–292.
- (22) Garbassi, F.; Occhiello, E. *J. Mater. Sci.* **1987**, *22*, 207–212.
- (23) Papirer, E.; Wu, D. Y.; Schultz, J. *J. Adhesion Sci. Technol.* **1993**, *7*, 343–362.
- (24) Kumar, S.; Singh, R.; Singh, T. P.; Sethi, B. L. *J. Mater. Process. Technol.* **2009**, *209*, 3675–3687.
- (25) Elson, J. M. *Phys. Rev. B* **1984**, *30*, 5460–5480.
- (26) Maradudin, A. A.; Mills, D. L. *Phys. Rev. B* **1975**, *11*, 1392–1415.
- (27) Church, E. L.; Jenkinson, H. A.; Zavada, J. M. *Opt. Eng.* **1979**, *18*, 125–136.
- (28) Patel, R.; Ratta, V.; Saavendra, P.; Li, J. *J. Plast. Film Sheet.* **2005**, *21*, 217–231.
- (29) Smith, P. F.; Chun, I.; Liu, G.; Dimitrievich, D.; Rasburn, J.; Vancso, G. J. *Polym. Eng. Sci.* **1996**, *26*, 2129–2134.
- (30) Ashizawa, H.; Spruiell, J. E.; White, J. L. *Polym. Eng. Sci.* **1984**, *24*, 1035–1042.
- (31) Briscoe, B. J.; Galvin, K. P. *Sol. Energy* **1991**, *46*, 191–197.